Preprints.org

Article

Exploring the Impact of Noise and Image Quality on Deep Learning Performance in Dxa Images

Dildar Hussain [*] and Yeong Hyeon Gu [*]

Article

Exploring the Impact of Noise and Image Quality on Deep Learning Performance in DXA Images

Dildar Hussain and Yeong Hyeon Gu *

Department of Artificial Intelligence and Data Science, Sejong University, Seoul 05006, Republic of Korea

* Correspondence: yhgu@sejong.ac.kr

Abstract: Background and Objective: Segmentation of the femur in Dual Energy X-ray (DXA) images poses challenges due to reduced contrast, noise, bone shape variations, and inconsistent X-ray beam penetration. In this study, we investigate the relationship between noise and certain deep learning (DL) techniques for semantic segmentation of the femur to enhance segmentation and bone mineral density (BMD) accuracy by incorporating noise reduction methods into DL models. **Methods:** Convolutional neural network (CNN) based models were employed to segment femurs in DXA images and evaluate the effects of noise reduction filters on segmentation accuracy and its effect on BMD calculation. Various noise reduction techniques were integrated into DL-based models to enhance image quality before training. We assessed the performance of the fully convolutional neural network (FCNN) in comparison to noise reduction algorithms and manual segmentation methods. **Results:** Our study demonstrated that FCNN outperformed noise reduction algorithms in enhancing segmentation accuracy and enabling precise calculation of BMD. The FCNN-based segmentation approach achieved a segmentation accuracy of 98.84% and a correlation coefficient of 0.9928 for BMD measurements, indicating its effectiveness in the clinical diagnosis of osteoporosis. **Conclusions:** In conclusion, integrating noise reduction techniques into DL-based models significantly improves femur segmentation accuracy in DXA images. The FCNN model, in particular, shows promising results in enhancing BMD calculation and clinical diagnosis of osteoporosis. These findings highlight the potential of DL techniques in addressing segmentation challenges and improving diagnostic accuracy in medical imaging.

Keywords: dual-energy X-ray absorptiometry (DXA); osteoporosis; deep learning; segmentation; FCN; noise; imperfection; filters

1. Introduction

Osteoporosis is a pathological condition that compromises the integrity of the skeletal system. It serves as the primary factor for hip fractures within many countries. It demonstrates an absence of gender discrimination and has the potential to materialize at any point during an individual's lifespan. A high proportion exceeding 20% of individuals affected with hip fractures succumb to the resultant trauma [1,2]. The disease can adequately be diagnosed with a low-dose X-ray imaging technique called dual-energy X-ray absorptiometry (DXA), which is considered a golden standard for diagnosing osteoporosis fracture risk [3]. Quantitative Computed Tomography (QCT) is another alternative. However, QCT requires a high dose of X-rays and is costly.

The initial step in precise osteoporosis involves accurate segmentation, which is crucial for ensuring the accurate calculation of bone mineral density (BMD) and final osteoporosis report generation. Segmentation errors can significantly impact the BMD calculation and subsequent analyses. However, several reasons drive incorrect segmentation in DXA images and post-analysis [4,5]. Firstly, the use of low-dose X-rays in DXA imaging provides noisy images. Secondly, there is an overlap of organs in human bodies. Thirdly, the irregular attenuation of the X-rays through the human body produces negative shadows, which appear as dark areas in the images. Other factors that affect segmentation quality include scanning orientation, luminous intensities, resolution, and variations between individuals [6,7].

Noise profoundly impacts medical imaging analysis, manifesting as artifacts, reduced image clarity, and potential misinterpretation of diagnostic information. It stems from diverse sources like

equipment limitations, patient motion, inadequate radiation doses, distorting image features, and complicating accurate identification and analysis of anatomical structures or pathologies. Moreover, noise undermines automated image processing algorithms, compromising segmentation, feature extraction, and classification tasks. Hence, effective noise reduction techniques are imperative for bolstering the accuracy and reliability of medical imaging analysis, thereby refining diagnostic interpretation and patient care [8,9].

In medical imaging, noise significantly disrupts segmentation processes by introducing inaccuracies and artifacts, hindering the precise delineation of anatomical structures. Obscured tissue boundaries due to noise often yield incomplete or erroneous segmentation results, while disrupted intensity gradients impede segmentation algorithms in distinguishing different regions of interest. Consequently, noise reduction techniques play a pivotal role in enhancing the accuracy and reliability of segmentation, ensuring meticulous delineation of structures, and maximizing the utility of imaging data for diagnostic and therapeutic endeavors [10–12].

Noise poses a substantial challenge to the performance of Deep Learning (DL) models in medical imaging by introducing uncertainties and inconsistencies in training data. Its presence obfuscates relevant features and patterns, leading to diminished model accuracy and reliability. Furthermore, noise exacerbates overfitting, wherein models learn to capture noise instead of meaningful information, impairing generalization to new data. Robust preprocessing techniques and noise reduction strategies are essential to mitigate these effects, improving training data quality and bolstering model performance. Additionally, the development of noise-robust architectures and training methods holds promise in enhancing model resilience to noise and variability in medical imaging data, ultimately augmenting their efficacy in clinical applications [13–15].

Regardless of the numerous techniques being used, accurate automatic segmentation in DXA imaging always remains a challenge [16–22]. Manual segmentation is time-consuming with the obligations of an expert, and unattainable for analyzing large public [16,18,19]. With the inherent limitations described in the references [23–25], the existing techniques are unsuitable for DXA image segmentation. All the limitations described in our previous work [26] forced us to new investigations, which led us to more precise segmentation with greater accuracy in DXA imaging.

Integration of denoising techniques into convolutional neural network (CNN) based DL models constitutes a critical step in the preprocessing pipeline. Before training, noisy DXA images undergo filtration using one or a blend of denoising methods to enhance their quality. These denoised images serve as input data for training the CNN model, enabling it to learn from cleaner and more representative image data. Subsequently, during inference, the trained CNN model is directly applied to noisy DXA images for femur segmentation, resulting in heightened accuracy and reliability in the segmentation process. To evaluate the impact of these denoising filters on DL-based image segmentation, we compiled the results by applying the CNN-based model to segment femur images and calculate BMD both with and without the application of denoising filters. This comparative analysis allows us to comprehensively understand the effectiveness of denoising techniques in enhancing the performance of DL-based segmentation algorithms. Preprocessing data (i.e., noise filters) and its effect on DXA image segmentation were not fully investigated previously, here in this study, we came up with the fact of preprocessing DXA images before they go to a DL modal.

We conduct comprehensive experiments to evaluate the effectiveness of the preprocessing steps and noise reduction effect over the recent DL-based approach for femur segmentation from DXA images. The best results were achieved with deeper fully convolutional neural network (FCNN) based architecture with a noise reduction filter using a nonlocal mean filter (NLMF) than previously applied techniques. We obtain both high-energy (HE) and low-energy (LE) images from a DXA scan. To create images with a high contrast, both are merged. We investigate the impact of preprocessing filters on noise or imperfections removal in high-contrast image creation, and consequently its effect on DL-based segmentation and BMD analysis.

The main objective of this research is to find a solution that improves the image segmentation, BMD calculation, and consequent analysis of DXA image analysis. The rest of the paper is organized

as follows. Section 2 explains the segmentation method of our model. Section 3 shows the proposed model results. Discussion about our method and results are presented in section 4. Section 5 presents some concluding remarks. Finally, Section 6 presents some future work to be carried out. The main contribution of this research is highlighted as follows:

- Advancement in DXA Imaging Segmentation: Introduces a DL approach with enhanced image quality with various image denoising techniques for femur segmentation, improving osteoporosis diagnosis and bone mineral density calculation accuracy.

- Application of DL in Medical Imaging: Expands FCNN use in DXA imaging, showing potential for addressing segmentation challenges and improving diagnostic accuracy.

- Future Research Directions: Identifies areas for improvement in femur segmentation, stimulating further inquiry and innovation in medical imaging and DL applications.

2. Methods

Data from the femur is obtained through DXA scanning, resulting in high-energy HE and low energy LE images. Before high-contrast images were produced from the combination of HE and LE photos, various denoising techniques were used to remove imperfections from HE and LE images.

With its exceptional accuracy and efficiency in tasks ranging from organ segmentation to illness diagnosis, DL has completely changed the field of medical image analysis. Femur segmentation from DXA images is one such crucial task that helps with osteoporosis diagnosis and tracking. However, several variables, such as noise and image quality, can affect how effective DL models are in this area. To create robust and dependable segmentation algorithms, it is essential to comprehend how noise and image quality affect DL performance.

2.1. Data Preparation

We utilized 600 femur images obtained by a DXA scanner (OsteoPro MAX, B.M.Tech Worldwide Co., Ltd., Republic of Korea). For model training, testing, and assessing the accuracy of DL techniques "ground truths" of manually segmented images and BMD results obtained by expert radiologists were collected for this study. Various denoising models were employed as a preprocessing step for high-contrast image generation and removal of imperfections from images. In the segmentation process, each pixel was categorized as either bone or soft tissue or air. For the five-fold evaluation test, the data were divided into two sets: 80% for training and 20% for independent testing. Subsequently, a test database was formed and fed into proposed DL-based modals lacking class labels, and the model generated output labels for each pixel of a test subject.

2.2. Image Generation

The domain of medical image analysis has witnessed recent advancements in DL techniques, which have demonstrated remarkable and state-of-the-art performance on vast datasets comprising numerous images across various categories. Nevertheless, these remarkable accomplishments underscore the susceptibility of different DL models to image quality concerns [27]. Thus, when considering DL models, image quality assumes a pivotal role. The enhancement of visual quality in images through contrast improvement and noise reduction can significantly impact image classification and segmentation [27–29]. In this investigative study, we acquire DXA data in the form of LE and HE images. These LE and HE images are merged to create a high-contrast display image, as depicted in **Figure 1** [30]. Our study aims to investigate the influence of three distinct types of high-contrast display images generated by DXA scans on the outcomes of DL. These high-contrast display images encompass images of bone density (IBD), image of HE, LE log ratio (ILR), and a collage image (CI). The IBD image, which serves as the initial output, can be generated by following these steps,

$$IBD = \frac{R_{st} \times \frac{\log HE_i}{HE_0} - \frac{\log LE_i}{LE_0}}{u_l - u_h \times R_{st}}, \tag{1}$$

$$R_{st} = \frac{\log \dfrac{LE_0}{\frac{1}{n}\sum_{i=1}^{n} LE_i}}{\log \dfrac{HE_0}{\frac{1}{n}\sum_{i=1}^{n} HE_i}}, \tag{2}$$

where u_l, u_h, are the constant value of a specific LE x-ray and HE x-rays respectively. HE_0 and LE_0 are incident energy at the source x-ray and HE_i, LE_i are detector counts at a specific scan location (i.e., image pixel). The BMD value at the bone region is always higher than the soft tissue region, therefore from equation 1, we get a brighter bone and darker soft tissue region image.

Figure 1. Acquire data with DXA machine scanning femur [30].

The second image we generate from raw DXA data is ILR, and can be generated as follows,

$$ILR = pow\left(T - \frac{\log(HE_i + LE_i)}{\log(u_l + u_h)}, B + C\right), \tag{3}$$

where T is a constant value and we used T=2.0 as a constant value. Similarly, B and C represent image brightness and contrast enhancement. We used B and C as constant values to be determined from experiments. Using equation 3 we get better contrasted images with clear boundaries between bone, soft tissue, and air than BMDI.

The third image we generate from DXA data is CI, and can be formed as follows,

$$CI = \left(\log\left(\frac{HE_i}{LE_i}\right) - \frac{\log\left(\frac{LE_i}{HE_i}\right)}{1 + e^{-\delta * \left(\log\left(\frac{LE_i}{HE_i}\right) - \mu\right)}}\right) * (B + C) - logLE_i, \tag{4}$$

where, 'δ' is the standard deviation (STD) of log (LE/HE) ratio and 'μ' is the mean of the log(LE/HE). The values of B and C represent image brightness and contrast values to be known from experiments. From equation 4 we get a very high contrast image with cleared boundaries between different regions (i.e., bone, soft tissues, and air) compared to IBD and ILR. As we see from **Figure 2** some information (most probably an artifact) pointed by red arrows in Figure 2 (a2) and (a3) are hidden which appear in CI and IBD images as pointed by red arrows in Figure 2 (c1) and (c3). So, CI gives a very highly contrasted image with detailed DXA scan information. One drawback of ILR image is that when an image contains an artifact the image appears very black as shown in Figure 2 (c2). This problem does not affect CI images as we see in Figure 2 (c3). We normalize the intensities of the image from 0 to 255 and the final image is saved in '.png' format to be used in the DL model.
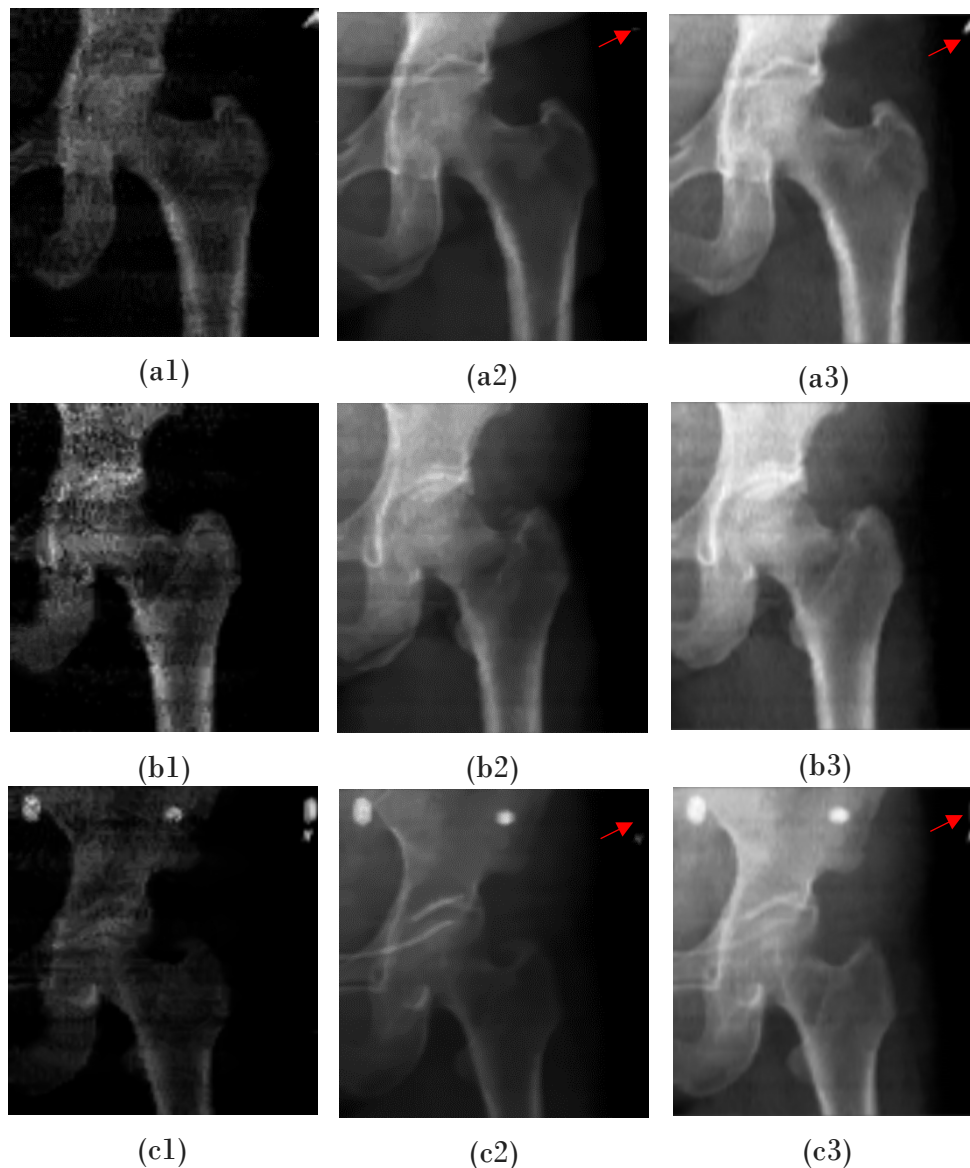
Figure 2. Generate high contrasted images from DXA scan.

2.3. Noise in DXA Images

DXA images, while widely used for bone density assessment, are susceptible to various forms of noise. These noises can originate from factors such as equipment imperfections, patient movement during imaging, or interference from surrounding objects. Common types of noise in DXA images include Gaussian noise, speckle noise, and motion artifacts. These noises can obscure important anatomical details and hinder accurate segmentation.

The presence of noise in DXA images can significantly affect the performance of DL models for femur segmentation. Noise introduces inconsistencies and irregularities in the image data, making it challenging for the model to distinguish between bone structures and background noise. As a result, DL algorithms may produce inaccurate segmentation, leading to erroneous clinical interpretations.

To mitigate the adverse effects of noise on DL performance in femur segmentation, various preprocessing techniques can be employed. These techniques include denoising algorithms such as Gaussian filtering, median filtering, or wavelet-based methods. Additionally, data augmentation strategies such as random rotations, translations, and elastic deformations can help improve the robustness of DL models to noise.

Denoising images is a very important preprocessing step in image classification and segmentation [28,29]. S. Calderon et al., studied the impact of denoising and contrast enhancement

using a deceived non-local means (DNLM) filter in a CNN-based approach for age estimation using digital hand X-ray images. The results they obtained results propose that both image contrast enhancement and denoising can remarkably improve the results in a CNN-based model [28]. Gabriel B et al., conducted a study about the effect of noise in image classification. Their study revealed that the image classification task was improved by the denoising process [29]. To improve the accuracy of image segmentation, noise reduction in both HE and LE images is an essential preprocessing procedure in DXA imaging. We employed and tested several denoising techniques such as Non-local Mean Filter (NLMF), Gaussian Filtering, and Wavelet-based denoising to check the improvement in segmentation and BMD calculation using DL-based segmentation. The NLMF eliminates noise by comparing the similarity of patches through pixel neighborhoods, Gaussian filtering involves convolving the DXA image with a Gaussian kernel. Similarly, Wavelet-based filtering in DXA imaging involves using wavelet transforms to analyze and process images.

2.3.1. Non-Local Mean Filter

The NLMF denoising technique is commonly used in medical imaging, including DXA imaging. In DXA imaging, where the images are often affected by noise due to factors such as low X-ray dose and scatter, denoising techniques like NLMF can be essential for improving image quality and enhancing the accuracy of subsequent analysis. Kim Kyuseok et al., (2020) [31] demonstrated through visual assessment and quantitative analysis that the NLM algorithm outperforms existing methods in processing casting images, offering an efficient solution to mitigate noise in high-energy X-ray imaging systems and potentially enhancing image restoration through accompanying software. Seungwan Lee et al., (2022) [32] introduce a newly improved non-local means (INLM) denoising algorithm tailored for X-ray images, accounting for the thickness of aluminum (Al) filters commonly used in X-ray systems, demonstrating its efficacy in reducing image noise. Results indicate that the proposed INLM algorithm, particularly when applied to X-ray images with a 5 mm Al filter thickness, exhibits superior performance in noise reduction and image evaluation compared to conventional methods, highlighting its importance for optimizing image processing applications in photon-counting X-ray systems.

The NLMF works by averaging the pixel values in an image, with the averaging process weighted based on the similarity between patches of pixels in the image. Unlike traditional filters that rely on local information, the NLM filter considers non-local similarities, meaning it compares patches of pixels from different image regions to determine the weighting for averaging. The approach of NLMF effectively removes noise while preserving image details, making it particularly suitable for medical imaging applications where preserving fine structures and details is crucial for accurate diagnosis and analysis. NLMF can help reduce the effects of noise, leading to clearer and more accurate DXA images, which in turn can improve the reliability of measurements such as BMD calculations and segmentation of bone structures.

The optimized NLMF is tested and verified with the DXA images of the uniform femur phantom and real human femur images. Preliminary results showed that signal-to-noise ratio (SNR) for high and low-energy femur DXA images improved by 15.26% and 13.55%, respectively. **Figure 3** shows some of the denoised results of femur DXA images using NLMF. More details about our NLMF work for denoising DXA images are available in references [33,34].
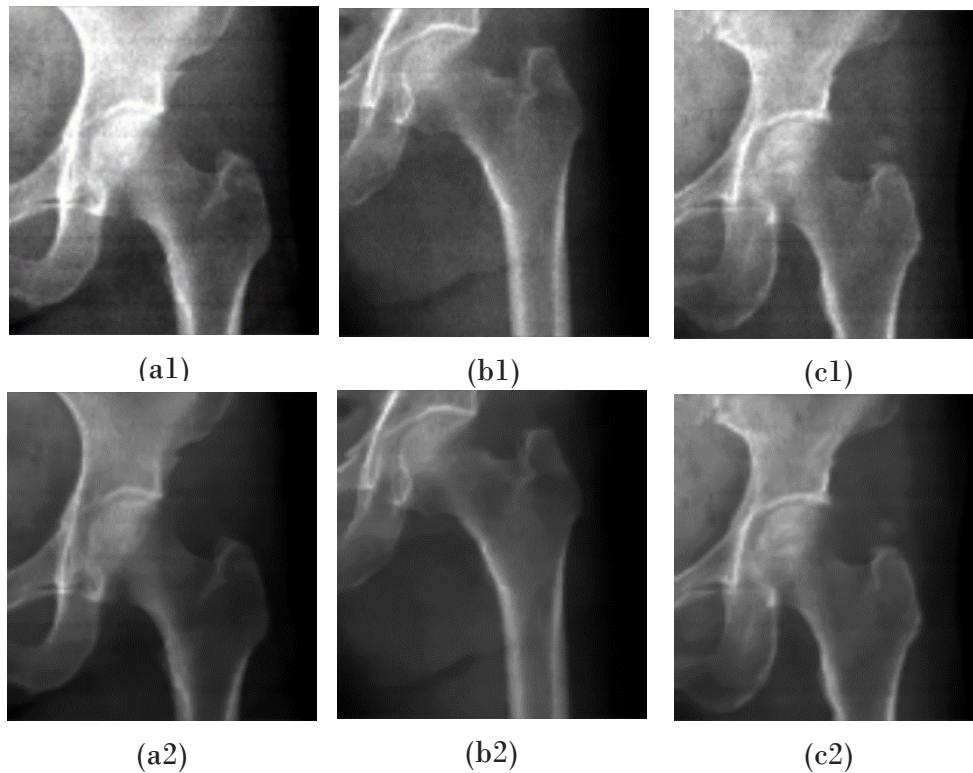
(a1)   (b1)   (c1)

(a2)   (b2)   (c2)

Figure 3. Denoising DXA images using NLMF.

2.3.2. Gaussian Filtering

Gaussian filtering (GF) is a common technique used for image processing and noise reduction. Gaussian filtering involves convolving the DXA image with a Gaussian kernel. This kernel is essentially a Gaussian distribution centered at the pixel of interest, with the values of neighboring pixels weighted according to their distance from the center. The Gaussian kernel is defined by its standard deviation, which determines the amount of smoothing applied to the image [35–38].

However, it's important to note that GF may also blur fine details in the image, so the choice of the filter's parameters (such as the standard deviation of the Gaussian kernel) should be carefully considered based on the specific requirements of the application. The equation for GF in DXA image processing can be expressed as:

$$G(i,j) = \frac{1}{2\pi\sigma^2} e^{-\frac{i^2+j^2}{2\sigma^2}*I(i,j)} \tag{5}$$

Where, G(i,j) is the filtered image, I(i,j) is the original image. σ is the standard deviation of the Gaussian distribution. This equation represents the convolution of the original image I(i,j) with a 2D Gaussian kernel. The Gaussian kernel is centered at (i,j) with values determined by the Gaussian function, where σ controls the width of the kernel and hence the amount of smoothing applied to the image.

Nazia Fathima et al., (2020) proposed a novel approach for accurately measuring BMD from X-ray images using a modified U-Net with Attention unit [39]. The proposed method includes preprocessing steps, including Gaussian filtering, to enhance image quality. Results demonstrate improved segmentation accuracy and high classification accuracy for osteoporosis detection, validating the effectiveness of the approach.

2.3.3. Wavelet-Based Methods

Wavelet-based denoising technique is octenyl practiced in medical imaging. Wavelet-based denoising decomposes medical images into different frequency components using wavelet transforms. High-frequency noise in the decomposed image is then suppressed through thresholding methods while preserving important diagnostic features. The denoised image is reconstructed, resulting in reduced noise and improved image quality suitable for clinical diagnosis and analysis [40,41]. G. Elaiyaraja et al., (2022) [42] Proposed an optimal wavelet threshold-based denoising filter effectively removes adaptive Gaussian noise from medical images, offering superior performance and efficiency. Farah Deeba et al., (2020) [43] proposed a Wavelet-based Mini-grid Network Medical Image Super-Resolution (WMSR) method that enhances low-resolution medical images by leveraging stationary wavelet transform (SWT). By combining wavelet sub-band images and utilizing sub-pixel layers, the model achieves superior performance in image reconstruction speed and quality.

Wavelet-based filtering in DXA imaging involves using wavelet transforms to analyze and process images [44,45]. Weiya Xie et al., (2021) [44] explored the application of photoacoustic time-frequency spectral analysis (PA-TFSA) for assessing bone mineral density (BMD) and structure. Utilizing wavelet transform-based PA-TFSA, simulations and experiments on bone samples reveal significant associations between frequency components and bone characteristics. Parameters derived from PA-TFSA, particularly mid band-fit and slope, demonstrate sensitivity in distinguishing between osteoporotic and normal bones.

Wavelet transforms are powerful tools for image processing because they can represent both frequency and spatial information simultaneously. The wavelet transform decomposes an image into different frequency components. It consists of two main components: the scaling function (approximation) and the wavelet function (detail). The wavelet transform can be applied in either one dimension (1D) or two dimensions (2D). The continuous wavelet transform (CWT) of a signal or image f(x) is defined as:

$$W(a,b) = \int_{-\infty}^{\infty} f(x)\emptyset_{a,b}(x)dx \tag{6}$$

Where, $\emptyset_{a,b}(x)dx$ is the wavelet function, scaled by a and translated by b.

In practice, continuous wavelet transformation is often computationally expensive. Therefore, the discrete wavelet transform (DWT) is commonly used. It decomposes the image into different scales and orientations, resulting in a multi-resolution representation of the image. DWT is applied iteratively to decompose the image into approximation (low-frequency) and detail (high-frequency) coefficients. This can be represented mathematically as:

$$W(j,k) = \sum_{n} s_{j,k}(n).\emptyset(n-k) \tag{7}$$

Where, W(j,k) are the wavelet coefficients at scale j and position k, $s_{j,k}(n)$ are the scalling cofficent, and Ø (n-k) is the wavelet function.

Wavelet-based denoising involves thresholding the wavelet coefficients to remove noise while preserving image details. This is achieved by setting coefficients below a certain threshold to zero. Common thresholding methods include hard thresholding and soft thresholding.
Hard Thresholding (HT):

$$T_H(x) = \begin{cases} x, & if\ |x| > T \\ & otherwise \end{cases} \tag{8}$$

Soft Thresholding (ST):

$$T_S(x) = sign(x).(|x| - T)_+ \tag{9}$$

Where T is the threshold value (.)+ denotes the positive part of the function.

2.1.3. Data Augmentation

DL algorithms necessitate a substantial volume of data for effective training. However, the limited size of medical datasets presents a significant challenge in this regard. To meet the large dataset requirements of deep neural network training the small data size is increased using data augmentation [35,36]. In this study, we addressed the data scarcity by randomly selecting 350 images and applying transformations such as image translations, and horizontal and vertical reflections, along with their subsequent scaling. These augmentations resulted in the expansion of our dataset to 1800 images, facilitating more robust training of deep neural networks.

2.2. Depp Learning Architecture

Figure 4 provides an overview of DXA image analysis employing DL methodologies. In this investigation, we introduce the U-Net, SegNet, and FCN approaches for femur segmentation from DXA images with preprocessing and postprocessing steps. The integration of pre- and post-processing step has been demonstrated to be crucial in significantly enhancing the efficacy of diverse tasks and applications. Through the utilization of pre-processing methodologies such as noise reduction, image standardization, and data enhancement, the original input data can be improved and optimized before its utilization in the model. These pre-processing approaches are employed to alleviate the impact of noise, variability, and discrepancies in the data to amplify the flexibility and precision of subsequent analyses or forecasts. Similarly, post-processing techniques like filtering, smoothing, and calibration can further perfect the outcomes generated by the model to ensure their alignment with specific quality or criteria. In essence, the incorporation of pre- and post-processing stages plays a pivotal role in maximizing the efficiency and efficacy of the entire data processing pipeline to attain exceptional performance outcomes.
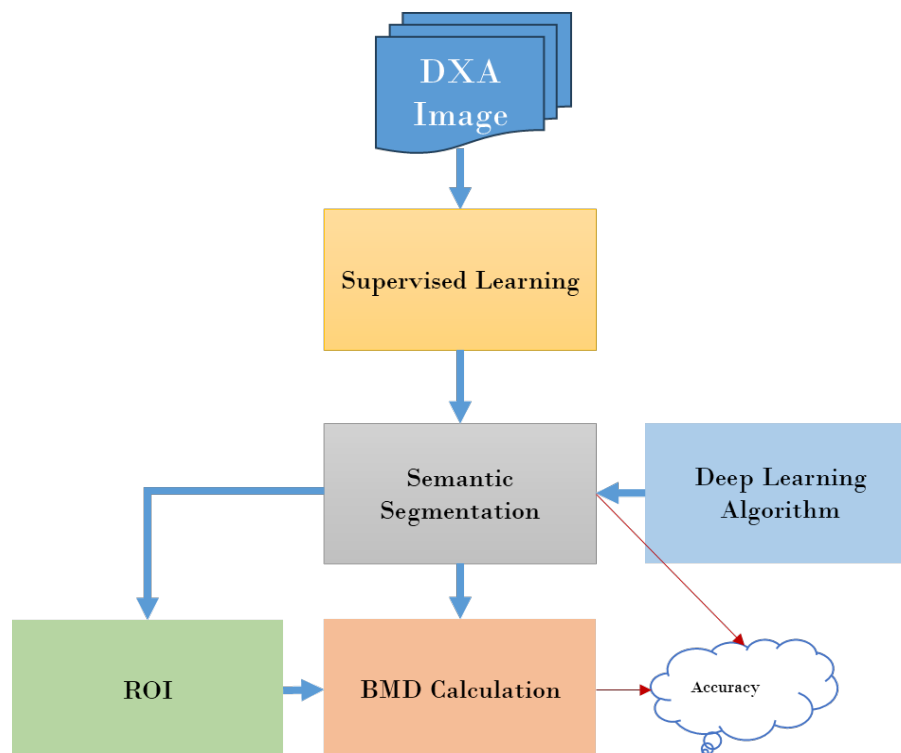

Figure 4. Overview of DXA image analysis using deep learning.

FCNs are adept at generating dense predictions from input data of variable dimensions. Notably, both training and inference processes operate on the entire image concurrently through dense feedforward computation and backpropagation [37]. Unlike conventional CNN models featuring fully connected layers (FCL), FCNs exclusively consist of convolutional layers without any FCL, as indicated by their names. Within the suggested DL segmentation networks, we employ the

sigmoid activation function in the activation layer to classify each pixel within the femur image into bone, soft tissue, or air categories. Further elaboration on the U-Net, SegNet, and FCN methodologies can be found in references [37–39]. The Adadelta optimization algorithm was employed to train all segmentation models, utilizing a batch size of 25. Initially, the learning rate was set to 0.2, with dynamic adjustments made throughout 200 epochs to optimize training. Weighted cross-entropy was utilized to compute the loss, aiming to minimize the overall loss H during the training phase as follows,

$$H = -\sum_{c=1}^{M} y_c log\,(\hat{y}_c)$$

(10)

where y represents the ground truth labels and $\hat{y}$ represents the predicted map of segmentation. M represents the number of classes and 'c' represents classes (bone, tissue, air). The research was implemented in Python utilizing the Keras framework, with TensorFlow serving as the backend library.

2.3. Post Processing

Unlike DL models, conventional semantic segmentation techniques typically necessitate the use of boundary smoothing filters to refine the femur bone boundaries delineated by the segmentation model and eliminate imperfections. In a prior investigation, we employed a binary smoothing filter to eradicate inaccuracies from segmented DXA images [23,24]. Addressing imperfections introduced during pixel labeling in image segmentation using machine learning is challenging. Morphological image processing (MIP) effectively handles these issues by considering the image's shape and structure. In instances where sometimes DL labeling of femur boundaries results in non-smooth contours, binary smoothing proves effective in refining femur object boundaries by eliminating small-scale noise while preserving large-scale features. For additional information regarding binary smoothing, please refer to our previous work cited in" [23,24].

2.4. Evaluation and Performance Analysis

To evaluate the performance of DL-based predictions with preprocessing noise filters compared to ground truth using a range of evaluation metrics. These metrics including True Positives (TP), True Negatives (TN), False Positives (FP), and False Negatives (FN), are recorded for each segmented pixel in the DXA image to quantify the accuracy of the models over the total number of pixels (n = TP + TN + FP + FN) in an image. These metrics were calculated over the entire dataset of test images.

One of the key evaluation metrics used in the study was Intersection over Union (IOU), which is a measure commonly used to assess the accuracy of segmented objects compared to ground truth. IOU is calculated as the ratio of the area of intersection between the segmented object and ground truth to the area of their union. This metric indicates how well the segmented object aligns with the ground truth, with higher IOU values indicating better alignment.

Additionally, Sensitivity (True Positive Rate, TPR) and Specificity (True Negative Rate, TNR) were used to measure the proportion of positive and negative pixels accurately identified, respectively. Sensitivity measures the proportion of bone tissue pixels correctly identified in the femur DXA image, while Specificity measures the proportion of soft tissue pixels correctly identified. False Positive Rate (FPR) and False Negative Rate (FNR) were also calculated to quantify the rate of misclassification of positive and negative pixels, respectively.

We employed a threshold-based approach to assess the overall accuracy of the segmentation methods. A segmentation method was considered successful if IOU was > 0.92, Sensitivity was greater > 95%, or Specificity was≥ 93%. These thresholds were chosen to ensure that the segmentation methods accurately identified both bone and soft tissue regions in the DXA images.

We used a five-fold cross-validation approach, by dividing the dataset as 80% for training, while the remaining 20% for independent testing. Test data were swapped with training data during cross-validation to ensure robust evaluation of the segmentation methods. Finally, segmentation methods retrieved ground truths (RGT) and manual ground truths (GT) were applied to the test data in each cross-validation fold to compare their performance. For more detail visit our previous work referenced in [References], as the same evaluation and performance analysis strategy was adopted to evaluate the accuracy of this work.

$$Accuracy = 100 \times \frac{1}{N} \sum_{i=1}^{N} x_i \; wher, f(x_i)$$

$$= \begin{cases} 0, & if \; JI < 0.92 \, || \varepsilon < 95 \, || \vartheta < 93 \\ 1, & else \end{cases}, \tag{11}$$

$$JI = \frac{TP}{TP + FP + FN}.$$

Where, in the above equation, JI is the Jaccard index or IOU, epsilons (ε) is the image segmentation sensitivity, and ϑ is the image segmentation specificity.

3. Results

3.1. Data

We used the same dataset used in our previous studies [23,24], with some additional femur images acquired on a DXA scanner (OsteoPro MAX, B.M.Tech Worldwide Co., Ltd., Republic of Korea). Radiology experts manually segmented femur images as the "ground truth". Manually annotated was extracted from the DXA system in the ".png" format along with high contrast images for training and testing our DL models. Each and every pixel in the femur image was annotated and assigned a class label (i.e., either bone, soft tissue, or air.

3.2. Noise Reduction

The proposed denoising techniques via NLMF, Gaussian Filtering and Wavelet-based methods for DXA images are evaluated experimentally with femur data. The performances of denoising filters have been evaluated quantitatively in terms of mean-to-standard deviation ratio (MSR), signal-to-noise ratio (SNR), and contrast-to-noise ratio (CNR). The proposed noise reduction techniques significantly improve the quality of DXA images and image segmentation results while preserving the fine details of anatomical structures. Compared to other denoising methods Wavelet-based filtering has shown higher performance in the case of the average improvement ratio of MSR, SNR, and CNR and improves the quality of DXA images. **Table 1** presents the effects of NLMF, GF and CWT filters. A sample of original and denoised images with NLMF is shown in **Figure 5.**
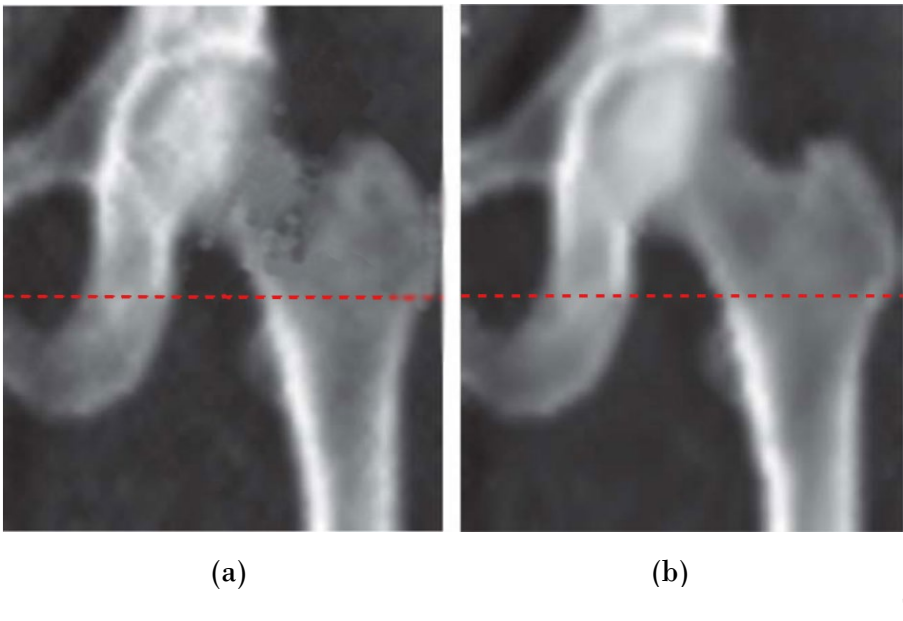
(a)   **(b)**

T

Figure 5. Image denoised with NLMF (a) original and (b) denoised image.

Table 1. Denoising techniques Performance analysis for femur DXA images. The results are presented in this table as mean values from all evaluated images.

Technique	Index	Image	
		Original	Denoised
NLMF	MSR	73.31	77.01
	SNR	5.26	5.74
	CNR	27.54	31.11
GF	MSR	73.31	74.15
	SNR	5.26	5.54
	CNR	27.54	29.26
CWT- HT	MSR	73.31	**78.21**
	SNR	5.26	**6.27**
	CNR	27.54	**32.63**
CWT- ST	MSR	73.31	77.81
	SNR	5.26	6.25
	CNR	27.54	31.41

3.3. Segmentation

This section presents the performance of U-Net, SegNet, and FCN approaches using test data (i.e., 250 femur images). Some of the selected results about U-Net, SegNet, and FCN output with non-smooth contours, and binary smoothed contours are shown in **Figure 6 and 7**, respectively. **Table 2** shows the segmentation performance results in terms of average accuracy computed using JI, sensitivity and specificity of all test images. A couple of the predicted segmentation contours by different segmentation models using NLMF are shown in **Figure 8**.
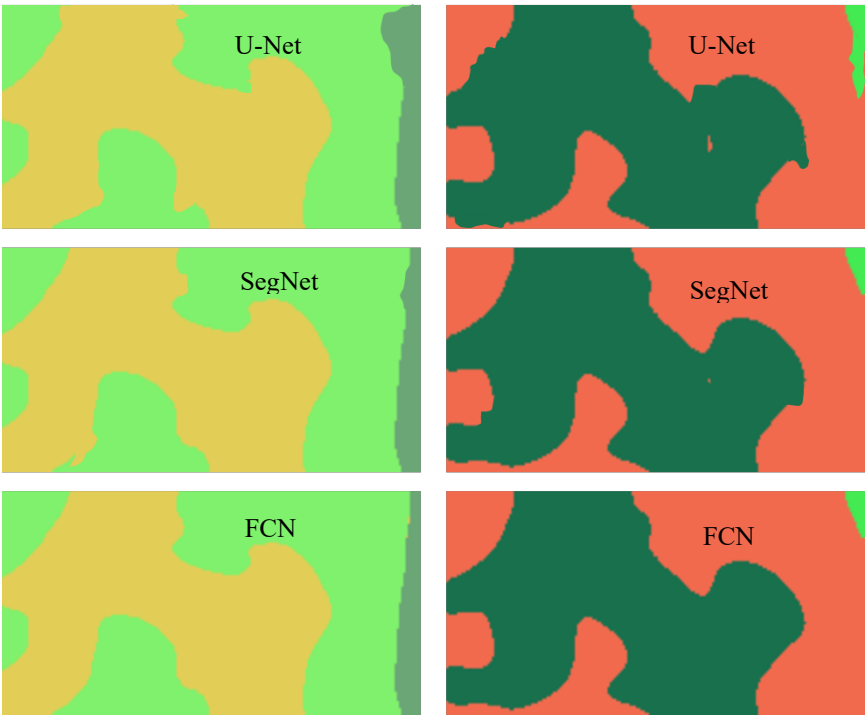
Figure 6. Selected results of two cases segmented with SegNet, U-Net, and FCN without smoothing filters.
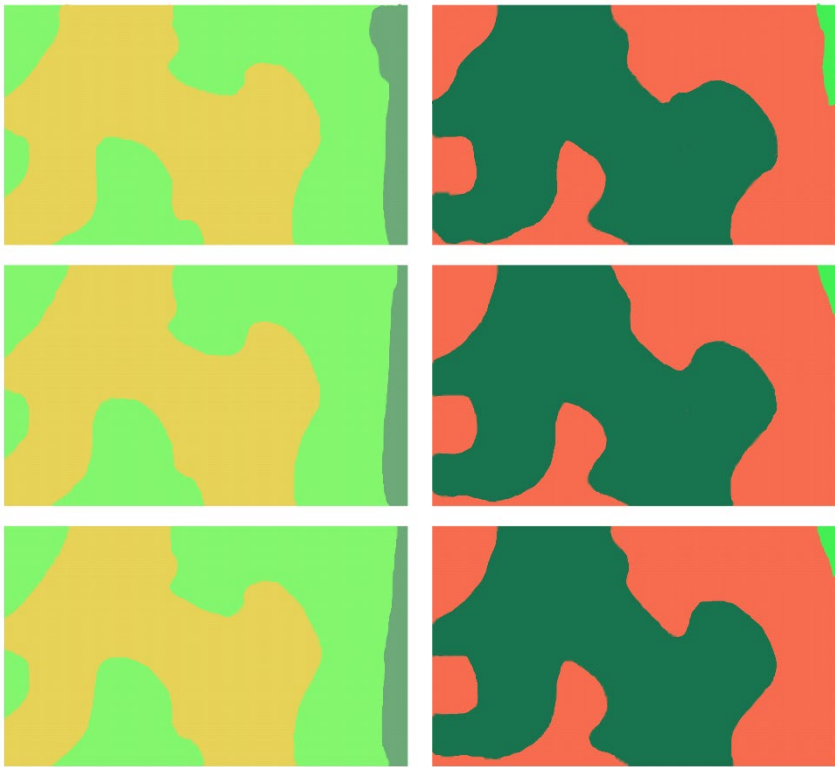

Figure 7. Selected results of two cases segmented with SegNet, U-Net, and FCN after using a binary smoothing filter.
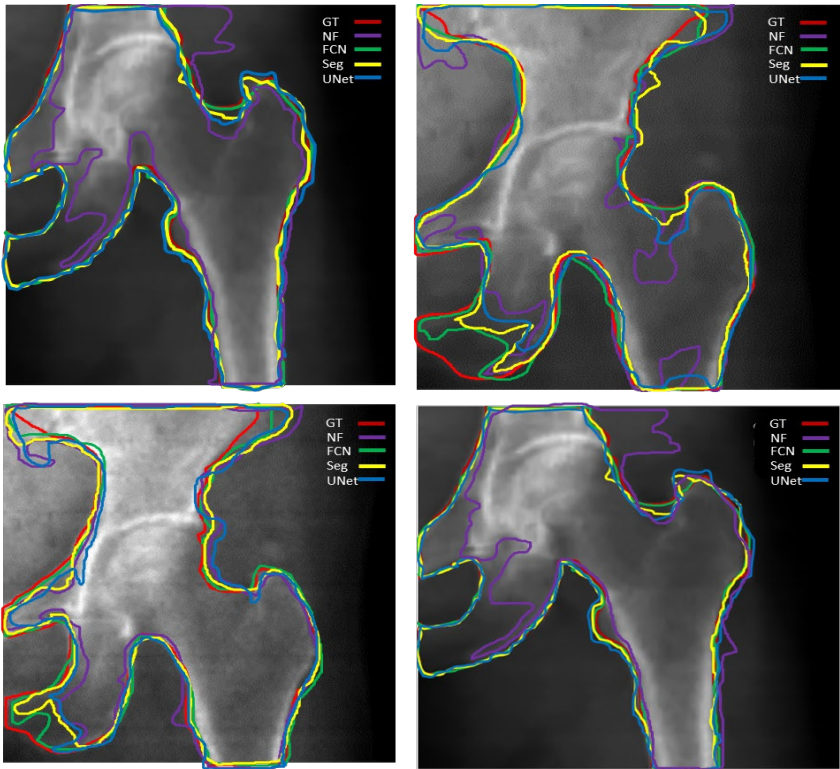
Figure 8. Predicted femur boundaries using SegNet, U-Net, and FCN segmentation models. Ground truth femur boundaries are outlined in red, while the predicted boundaries are represented by yellow (SegNet), blue (U-Net), green (FCN) and purple (No filter). The above segmentation results were obtained following a preprocessing with NLMF.

Table 2. Segmentation performance of different methods on the test dataset.

DL Model	Trainable Parameters	Loss Function	Optimization Algorithm	Pre-processing (Denoising Method)	Segmentation Accuracy (%)
SegNet				No pre-processing	88.12
				NLMF	92.99
	13.3M	Cross-Entropy	Adam	GF	92.35
				CWT- HT	96.63
				CWT- ST	93.68
U-Net				No pre-processing	86.32
				NLMF	91.56
	12.7M	Dice Loss	Adam	GF	89.98
				CWT- HT	94.14
				CWT- ST	91.89
FCN				No pre-processing	89.36
				NLMF	94.76
	134.5M	Cross-Entropy	Adam	GF	93.89
				CWT- HT	**98.84**
				CWT- ST	94.97

Segmenting femur images yielded significantly higher accuracy (98.84%) when employing FCN with CWT-HT techniques and incorporating a binary smoothing filter to refine object boundaries

compared to other segmentation models. Optimal results were achieved by fine-tuning FCN with CWT as a preprocessing tool for DXA data. In our evaluation of 250 test femur images segmented using FCN and other DL models, each model demonstrated superior performance compared to conventional methods, particularly in high-contrast femur sections (femur head and shaft) and challenging areas (greater and smaller trochanteric). The data was collected on multiple devices, and models well covered the diversity and performed competently.

3.4. BMD Analysis

We conducted a comparison of BMD between manually segmented images and those segmented by our models. Initially, a set of 100 femur images was randomly chosen and given to three individuals to manually segment the femur, select regions of interest (ROIs), and calculate BMD at three distinct regions: the femur neck, ward, and greater trochanter (G.T.). Subsequently, the average BMD value was computed from the three expert readings for each region, and these estimations were then compared to those obtained through model-based segmentation to assess consistency. Finally, we conducted a statistical analysis, calculating the Coefficient of Determination R^2, to evaluate the correlation of BMD measurements between different segmentation methods and manual segmentation. The FCN segmentation method with a CWT as preprocessing and binary smoothing of object boundaries as a post-processing step exhibited the highest correlation, as indicated in **Table 3**.

The findings underscore the superior "sensitivity, specificity, and accuracy" of the FCN method with preprocessing and postprocessing steps compared to other models, providing a robust solution for segmentation challenges in DXA imaging. While CNN is acknowledged as an innovative segmentation method, its reliance on large training datasets poses a limitation. To address this, we implemented transfer learning to enhance the training efficiency of DL models using small femur DXA images. Leveraging the weights of the pre-trained VGG-16 network from the extensive ImageNet dataset, our study on femur segmentation demonstrates that current DL models outperform previously utilized methods [23–26].

Training CNN-based networks with limited data poses a significant challenge in DL. Without optimized techniques and data augmentation, achieving satisfactory performance can be daunting. Therefore, employing appropriate optimization methods, data augmentation strategies, and transfer learning can greatly aid in training a reliable segmentation network. Transfer learning involves fine-tuning a deep network that has been pre-trained on either medical images or general datasets. When combined with data augmentation, transfer learning offers an additional distinct solution with numerous parameters. To tackle this challenge effectively, we successfully implemented transfer learning in our DXA image analysis, leveraging pre-trained models from ImageNet to enhance performance.

Table 3. Correlation record of BMD measurements between different segmentation methods to manual segmentation.

DL Model	Denoising Method	R²			
		Neck	Ward	G.T.	Mean
SegNet	Without Noise filter	0.9029	0.9108	0.9192	0.9109
	NLMF	0.9819	0.9798	0.9592	0.9736
	GF	0.9231	0.9307	0.9382	0.9306
	CWT- HT	0.9331	0.9467	0.9481	0.9426
	CWT- ST	0.9288	0.9348	0.9421	0.9352
U-Net	Without Noise filter	0.8929	0.9018	0.8892	0.8946
	NLMF	0.9811	0.9896	0.9560	0.9755
	GF	0.8989	0.9102	0.9013	0.9034

	CWT- HT	0.9601	0.9634	0.9418	0.9551
	CWT- ST	0.9599	0.9595	0.9388	0.9527
	Without Noise filter	0.9413	0.9349	0.9324	0.9362
	NLMF	0.9698	0.9789	0.9814	0.9767
FCN	**GF**	0.9479	0.9398	0.9404	0.9427
	CWT- HT	**0.9913**	**0.9949**	**0.9924**	**0.9928**
	CWT- ST	0.9734	0.9829	0.9816	0.9795

During the correlation statistical analysis of femur BMD measurement, we found a significantly higher correlation ($R2 = 0.9928$) between measurements from FCN segmented to expert segmented femur images with the CWT preprocessing technique. Additionally, a binary smoothing filter was employed as a postprocessing step along with CWT. Further investigations may discover the rational serviceability of FCN and other DL models in the clinical diagnosis of osteoporosis and the prediction of fracture risk. All DL-based models have proven to have better performance than previously applied techniques. The study has shown that convolutional networks can effectively be utilized with high performance on a small clinical data set using transfer learning in semantic segmentation.

4. Discussion

The study investigated the influence of noise and image quality on the performance of DL models for femur segmentation from DXA images. A dataset comprising DXA images with varying levels of noise and image quality was utilized to assess the effectiveness of different denoising techniques in improving segmentation accuracy.

Firstly, the impact of noise on segmentation performance was evaluated. DXA images with simulated Gaussian noise at different levels were subjected to segmentation using a baseline CNN model. Results demonstrated a noticeable decrease in segmentation accuracy with increasing noise levels. However, when denoising techniques such as Gaussian filtering, CWT filtering, and Non-local Mean Filter were applied as preprocessing steps, the segmentation accuracy improved significantly across all noise levels. Particularly, the Wavelet-based Mean Filter exhibited the highest efficacy in reducing noise and enhancing segmentation accuracy.

Secondly, the influence of image quality on segmentation performance was analyzed. DXA images with varying levels of blur and contrast were utilized to assess the robustness of the CNN model to image quality variations. It was observed that images with low contrast and blur presented challenges for the CNN model, leading to decreased segmentation accuracy. Nevertheless, by applying preprocessing techniques such as contrast enhancement and Wavelet-based filtering, the model demonstrated improved performance in segmenting femur structures from low-quality images.

Furthermore, the combined effect of noise and image quality on segmentation performance was investigated. DXA images with simultaneous variations in noise and image quality were used to simulate real-world scenarios. The results indicated that denoising techniques played a crucial role in mitigating the adverse effects of both noise and low image quality on segmentation accuracy. Wavelet-based methods, in particular, exhibited robust performance in preserving image details while reducing noise, resulting in improved segmentation accuracy even in challenging imaging conditions.

Image denoising plays a crucial role in enhancing the performance of CNN-based DL models, particularly in medical image analysis tasks such as femur segmentation from DXA images. Various denoising techniques, including Non-local Mean Filter, Gaussian filtering, Median filtering, and Wavelet-based methods, contribute to improving the robustness and accuracy of CNN models by reducing the impact of noise on image data.

Incorporating FCN-based segmentation with a preprocessing filter of Wavelet-based, and a binary smoothing filter as a postprocessing step, we observed a significant enhancement in femur

segmentation accuracy and BMD calculation in DXA images. Our findings demonstrated that FCN, when coupled with Wavelet-based, outperformed alternative segmentation techniques, achieving a notable accuracy rate. The application of Wavelet-based filtering as a preprocessing step effectively reduced noise and enhanced image quality, thereby facilitating more precise femur segmentation in DXA imaging. Furthermore, the combination of FCN and Wavelet-based exhibited robust performance across a range of imaging conditions, including challenging regions like the greater and smaller trochanteric areas, as well as high-contrast regions such as the femur head and shaft. These results underscore the potential of FCN-based segmentation with Wavelet-based filtering as a reliable approach for accurate femur segmentation in DXA imaging, offering superior sensitivity, specificity, and overall accuracy compared to traditional methods.

The results highlight the significance of incorporating denoising techniques into CNN-based DL models for femur segmentation from DXA images. By effectively mitigating the influence of noise and image quality variations, these techniques enhance the accuracy and reliability of segmentation, facilitating more precise diagnosis and monitoring of osteoporosis.

5. Conclusion

Segmentation of the femur in DXA images poses challenges due to factors like reduced contrast, noise, and variations in bone shape. This study investigated the impact of noise on DL techniques for femur segmentation, incorporating noise reduction techniques to enhance DL-based models' accuracy. By applying CNN to DXA images with and without noise reduction filters, we observed that the FCNN outperformed the use of noise reduction algorithms before model training, resulting in precise bone density calculation and improved osteoporosis diagnosis. The study demonstrated a higher accuracy of 98.84 % for different segmentation methods and a significantly higher correlation ($R2 = 0.9928$) for BMD measurement compared to manual segmentation. This research contributes to advancing DXA imaging segmentation, enhancing diagnostic accuracy, and stimulating further inquiry into medical imaging and DL applications. The incorporation of Non-local Mean Filter, Gaussian filtering, and Wavelet-based methods for image denoising in CNN-based DL models significantly contributes to improving the performance and robustness of femur segmentation from DXA images, ultimately enhancing the quality of osteoporosis diagnosis and patient care.

6. Future Directions

In the realm of medical imaging, future directions for femur segmentation from DXA images encompass several promising avenues. One avenue involves delving into advanced denoising techniques, such as deep learning-based models or adaptive algorithms, to further refine noise reduction strategies and enhance the accuracy of segmentation. Additionally, exploring the fusion of DXA images with other modalities like MRI or CT scans could unlock synergistic benefits, improving segmentation accuracy by leveraging complementary information from diverse imaging sources. Transfer learning and domain adaptation techniques offer another promising pathway, enabling model training on diverse datasets and enhancing generalization to different imaging conditions and patient populations. Moreover, developing methods for uncertainty quantification could provide valuable insights into the reliability of segmentation results, facilitating more informed decision-making in clinical settings. Clinical validation studies are essential for assessing the real-world performance and clinical utility of DL-based segmentation models, necessitating collaboration with medical professionals and institutions for rigorous validation against ground truth annotations and clinical outcomes. User-friendly software tools and platforms for DXA image segmentation should be developed to streamline integration into existing medical workflows and promote widespread adoption. Longitudinal studies exploring the prognostic value of segmentation-based biomarkers for predicting clinical outcomes, such as fracture risk or treatment response, offer valuable insights into personalized risk assessment and treatment planning in osteoporosis management. Lastly, addressing ethical considerations and potential biases in DXA image segmentation is paramount for ensuring equitable and unbiased healthcare delivery, requiring robust strategies for bias mitigation, fairness assessment, and transparency in model development and deployment.

References

1. K.M.Karlsson, I.Sernbo, K. Obrant, I.Redlund-Johnell and O.Johnell, "Femoral neck geometry and radiographic signs of osteoporosis as predictors of hip fracture," Bone 18, no. 4 (1996), 327-330., vol. 18, no. 4, pp. 327-330, 1996.

2. K. Holvik, C. Ellingsen, S. Solbakken, T. Finnes, O. Talsnes, G. Grimnes, G. Tell, A. Søgaard and H. Meyer, "Cause-specific excess mortality after hip fracture: the Norwegian Epidemiologic Osteoporosis Studies (NOREPOS)," BMC geriatrics, vol. 23, no. 1, p. 201, 2023.

3. E. Ghalenavi, Z. Mirfeizi, K. Hashemzadeh, M. Sahebari and M. Joker, "Diagnostic Value of Radiographic Singh Index Compared to Dual-Energy X-Ray Absorptiometry Scan in Diagnosing Osteoporosis: A Systematic Review," Archives of Bone and Joint Surgery, vol. 12, no. 1, p. 1–11, 2024.

4. R. Dendere, J. Potgieter, S. Steiner, S. P. Whiley and T.S. Douglas, " Dual-Energy X-ray Absorptiometry for Measurement of Phalangeal Bone Mineral Density on a Slot-Scanning Digital Radiography System," IEEE Transactions on Biomedical Engineering , vol. 62, no. 12, pp. 2850-2859, 2015.

5. N. Peel, A. Johnson, N. Barrington, T. Smith and D. R. Eastell, "Impact of anomalous vertebral segmentation on measurements of bone mineral density," Journal of Bone and Mineral Research, vol. 8, no. 6, pp. 719-723, 1993.

6. C. CriŞan and S. Holban, "A comparison of X-ray image segmentation techniques," Advances in Electrical and Computer Engineering, vol. 13, no. 3, pp. 85-92, 2013.

7. S. Fathima, R. Tamilselvi, M. Beham and A. Nagaraj, " A deep learning approach on segmentation of bone for bmd measurement from dexa scan images," in 2020 Sixth International Conference on Bio Signals, Images, and Instrumentation (ICBSII), Chennai, India, 2020.

8. M. Sanchez, M. Sánchez, V. Vidal, G. Verdu, G. Verdú, P. Mayo and F. Rodenas, "Medical image restoration with different types of noise," in 2012 Annual International Conference of the IEEE Engineering in Medicine and Biology Society, San Diego, California, USA, 2012.

9. B. Goyal, S. Agrawal and B. Sohi, "Noise issues prevailing in various types of medical images," Biomedical & Pharmacology Journal, vol. 11, no. 3, p. 1227, 2018.

10. K. V. Vijaya and V. Kalpana, "Effect of noise on segmentation evaluation parameters," in Soft Computing: Theories and Applications: Proceedings of SoCTA 2019, Singapore: Springer Singapore, 2020.

11. D. Tenbrinck and X. Jiang, " Image segmentation with arbitrary noise models by solving minimal surface problems," Pattern Recognition, vol. 48, no. 11, pp. 3293-3309, 2015.

12. T. Chen, C. Wang and H. Shan, "Berdiff: Conditional bernoulli diffusion model for medical image segmentation," in International Conference on Medical Image Computing and Computer-Assisted Intervention, Cham: Springer Nature Switzerland, 2023.

13. F. Khalid, M. Hanif, S. Rehman, J. Qadir and M. Shafique, "Fademl: Understanding the impact of pre-processing noise filtering on adversarial machine learning," in 2019 Design, Automation & Test in Europe Conference & Exhibition (DATE), IEEE, Firenze Fiera in Florence, Italy, 2019.

14. K. Maharana, S. Mondal and B. Nemade, "A review: Data pre-processing and data augmentation techniques," Global Transitions Proceedings, vol. 3, no. 1, pp. 91-99, 2022.

15. T. Dhar, N. Dey, S. Borra and R. Sherratt, "Challenges of deep learning in medical image analysis—Improving explainability and trust," IEEE Transactions on Technology and Society, vol. 4, no. 1, pp. 68-75, 2023.

16. K. E. Naylor, E. V. McCloskey, R. Eastell and L. Yang, "Use of DXA-based finite element analysis of the proximal Femur in a longitudinal study of hip fracture," Journal of Bone and Mineral Research, vol. 28, no. 5, pp. 1014-1021, 2013.

17. T. A. Burkhart, K. L. Arthurs and D. M. Andrews, "Manual segmentation of DXA scan images results in reliable upper and lower extremity soft and rigid tissue mass estimates," Journal of Biomechanics, vol. 42, no. 8, pp. 1138-1142, 2009.

18. H. Yasufumi, Y. Kichizo, F. M. I. Toshinobu, T. Kichiya and N. Yasuho, "Assessment of bone mass by image analysis of metacarpal bone roentgenograms: a quantitative digital image processing (DIP) method," Radiation medicine, vol. 8, no. 5, pp. 173-178, 1990.

19. C. Matsumoto, K. Kushida, K. Yamazaki, K. Imose and T. Inoue, "Metacarpal bone mass in normal and osteoporotic Japanese women using computed X-ray densitometry," Calcified tissue international, vol. 55, no. 5, pp. 324-329, 1994.

20. J. P. Wilson, K. Mulligan, B. Fan, J. L. Sherman, E. J. Murphy, V. W. Tai and C. L. Powers, "Shepherd, Dual-energy X-ray absorptiometry–based body volume measurement for 4-compartment body composition," The American journal of clinical nutrition, vol. 95, no. 1, pp. 25-31, 2012.

21. M. Roberts, T. Cootes, E. Pacheco and J. Adams, "Quantitative vertebral fracture detection on DXA images using shape and appearance models," Academic radiology, vol. 14, no. 10, pp. 1166-1178, 2007.

22. N. Sarkalkan, H. Weinans and A. A. Zadpoor, "Statistical shape and appearance models of bones," Bone, vol. 60, pp. 129-140, 2014.

23. D. Hussain and S. Han, "Computer-aided osteoporosis detection from DXA imaging," Computer methods and programs in biomedicine, vol. 173, pp. 87-107, 2019.

24. D. Hussain, Al-Antari, A.-M. M. M.A., S. Han and T. Kim, "Femur segmentation in DXA imaging using a machine learning decision tree," ournal of X-ray Science and Technology, vol. 26, no. 5, pp. 727-746, 2018.

25. D. Hussain, S. Han and T. Kim, "Automatic hip geometric feature extraction in DXA imaging using regional random forest," Journal of X-ray Science and Technology, vol. 27, no. 2, pp. 207-236, 2019.

26. D. Hussain, R. Naqvi, W. Loh and J. Lee, "Deep learning in DXA image segmentation," Computers, Materials & Continua, vol. 63, no. 3, pp. 2587-2598, 2021.

27. D. Samuel and L. Karam, "Understanding how image quality affects deep neural networks," in Quality of Multimedia Experience (QoMEX), 2016 Eighth International Conference, IEEE, Lisbon, Portugal, 2016.

28. S. Calderon, F. Fallas, M. Zumbado, P. N. Tyrrell, H. Stark, Z. Emersic, B. Meden and M. Solis, "Assessing the Impact of the Deceived Non Local Means Filter as a Preprocessing Stage in a Convolutional Neural Network Based Approach for Age Estimation Using Digital Hand X-Ray Images," in 2018 25th IEEE International Conference on Image Processing (ICIP), IEEE, Athens, Greece, 2018.

29. G. B. P. Costa, W. A. Contato, T. S. Nazare, J. E. Neto and M. Ponti, "An empirical study on the effects of different types of noise in image classification tasks," arXiv preprint arXiv:1609.02781, pp. 1-6, 9 Sep 2016.

30. M. Eric Chehab, "Illinois Bone & Joint Institute. (n.d.)," Osteoporosis Podcasts, [Online]. Available: https://www.ibji.com/podcasts/osteoporosis/. [Accessed 6 March 2024].

31. K. Kim, J. Choi and Y. Lee, "Effectiveness of non-local means algorithm with an industrial 3 mev linac high-energy x-ray system for non-destructive testing," Sensors, vol. 20, no. 9, p. 2634, 2020.

32. S. Lee and Y. Lee, "The impact of improved non-local means denoising algorithm on photon-counting X-ray images using various Al additive filtrations," Nuclear Instruments and Methods in Physics Research Section A: Accelerators, Spectrometers, Detectors and Associated Equipment, vol. 1027, p. 166244, 2022.

33. M. A. Al-antari, M. A. Al-masni, M. Metwallyb, D. Hussain, S. J. Parkb, J. S. Shinb, S. M. Hana and T. S. Kima, "Denoising images of dual energy X-ray absorptiometry using non-local means filters," Journal of X-ray Science and Technology, vol. 26, no. 3, pp. 395-412, 2018.

34. M. A. Al-Antari, M. A. Al-Masni, M. Metwally, D. Hussain, E. Valarezo, P. Rivera, G. Gi, J. M. Park, T. Y. Kim, S. J. Park, J. S. Shin, S. M. Han and T. S. Kim, "Non-local means filter denoising for DXA images," in Engineering in Medicine and Biology Society (EMBC), 39th Annual International Conference of the IEEE, Jeju Island, Korea, 2017.

35. S. Kaur, R. Hooda, A. Mittal, Akashdeep and S. Sofat, "Deep CNN-based method for segmenting lung fields in digital chest radiographs," in Advanced Informatics for Computing Research: First International Conference, ICAICR 2017, Springer Singapore, Jalandhar, India, March 17–18, 2017.

36. A. Krizhevsky, I. Sutskever and G. E. Hinton, "ImageNet classification with deep convolutional neural networks," Communications of the ACM, vol. 60, no. 6, pp. 84-90, 2017.

37. E. Shelhamer, J. Long and T. Darrell, "Fully convolutional networks for semantic segmentation," IEEE transactions on pattern analysis and machine intelligence, vol. 39, no. 4, pp. 640-651, 2017.

38. O. Ronneberger, P. Fischer and T. Brox, "U-net: Convolutional networks for biomedical image segmentation," in International Conference on Medical Image Computing and Computer-Assisted Intervention, Springer International Publishing, Munich, Germany, 2015.

20

39. V. Badrinarayanan, A. Kendall and R. Cipolla, "Segnet: A deep convolutional encoder-decoder architecture for image segmentation," in arXiv preprint arXiv:1505.07293, 2015.
40. OpenAI, "ChatGPT-3.5," Microsoft Corporation, [Online]. Available: https://chat.openai.com/. [Accessed 1-30 March 2024].